Superconducting Spin Valves Based on a Single Spiral Magnetic Layer

N.G. Pugach, M.O. Safonchik, V.I. Belotelov, T. Ziman, Thierry Champel

Superconducting spin valve under magnonic control

N. G. Pugach
HSE University, 101000, Moscow, Russia

M. O. Safonchik
A. F. Ioffe Physical-Technical Institute, RU-194021, St Petersburg, Russia

V. I. Belotelov
Lomonosov Moscow State University, Leninskie Gory 1(2), 119991, Moscow, Russia and
V.I. Vernadsky Crimean Federal University, Vernadsky Prospekt, 4, Simferopol 295007, Crimea

T. Ziman
Institut Laue-Langevin, BP 156, 41 avenue des Martyrs, 38042 Grenoble Cedex 9, France

T. Champel
Univ. Grenoble Alpes, CNRS, LPMMC, 38000 Grenoble, France
(Dated: October 1, 2021)

The detailed investigation of a superconducting spin-triplet valve is presented. This spin valve consists of a superconducting film covering a metal with intrinsic spiral magnetic order, which may be the result of a competitive exchange or of an asymmetric Dzyaloshinsky-Moriya exchange following from the central symmetry breaking of the crystal lattice. Depending on the anisotropy, this metal may change its magnetization either from a spiral to uniform order, as in Ho and Er, or in the direction of the spiral itself, as in B20 family crystals. Very recently, a new way of controlling the superconducting spin valve has been developed: the change of the magnetic order may also be triggered by magnonic relaxation processes, thus merging superconducting spintronics and magnonics. The nonuniform magnetic order controls the appearance of long-range triplet superconducting correlations (LRTC), which change the conditions of the proximity effect, enabling an external magnetic control of the superconducting critical temperature. We show that magnetic control of the spin-valve behavior can also be obtained for moderately low exchange energies thanks to an orientation-dependent averaging mechanism of the magnetic inhomogeneity on the scale of the Cooper pairs. The competition between these two mechanisms yields different behaviors of the spin-valve effect. Our numerical calculations show that at low exchange fields (as in MnSi) the spin valve effect may be quite significant. They suggest the switching behavior of the superconducting spin valve to be better optimized for B20 family compounds allowing magnonic control.

I. INTRODUCTION

Superconducting spintronics is a relatively new field in cryogenic nanoelectronics [1] appeared since 2010s [2]. As in traditional spintronics, the approach is to utilize spin transfer for information processing. Since a spin current is not always accompanied by a charge transfer, such devices combining magnetic and superconducting orders promise to be energy efficient. This new field is currently in development with the demonstration of new device concepts [3–5]. Magnetic control of charge transfer is the main mechanism of spintronic devices work and, in particular, of magnetic memory (MRAM) unit cells functionality. Like traditional MRAM elements based on magnetic tunnel junctions and spin transfer torque elements, superconducting spin valves (SSVs) were developed first theoretically [6–8], and are currently at the stage of optimization [9–11].

The magnetization reversal of a ferromagnetic element (F) may provide for magnetic control of the Josephson current [12–15] or may change the superconducting critical temperature T_c both in the F/S/F [16] and S/F/F [17] configurations, where S is a superconducting film. The possibility to tune superconductivity by the mutual orientation (parallel or antiparallel) of two F layers in this type of SSVs was shown in different experiments [18–21]. The shift δT_c in the critical temperature was assumed to be due to the paramagnetic effect, i.e., the breaking of the Cooper pairs by the spin polarizations induced into the S layer from the F layers. When the magnetization in the F layers are antiparallel, these polarizations effectively cancel out, while in the parallel configuration the induced polarizations act cooperatively to suppress superconductivity.

Later, the triplet mechanism of SSV effect was detected in the same structures. It was shown that a noncollinear magnetization configuration may even provide a larger δT_c shift [9, 22, 23] due to the appearance of long range triplet superconducting correlations (LRTC) [24–27]. The production of the LRTC, which can be seen as a new channel for the draining of the Cooper pairs from the superconductor, enhances the proximity effect, and therefore, efficiently reduces T_c. A full T_c switch, where δT_c is larger than the superconducting transition width, has been achieved in a few experiments [28–31].

Nevertheless, the improvement and optimization of SSVs still remains both a theoretical and experimental challenge [32–38]. The possible ways to improve the SSV properties call for the optimization of the structures, via their technology of preparation, quality of interfaces, and choice of materials, including strong, half-metallic, and insulating ferromagnets.

Recently, layers of the spiral magnet (M) holmium have been used as spin-mixers, improving magneto-resistive properties of SSVs [9, 39–44]. Taken separately in a S/M bilayer, a spiral or conical magnetic layer also provides a T_c shift under the action of an external magnetic field [44, 45]. Indeed, a parallel magnetization of the spiral magnetic layer suppress the LRTC that leads to a change in T_c. However, the return to the initial helimagnetic state requires a heating of the sample above the Curie temperature (much higher than T_c), what makes this kind of SSVs difficult to use in low-temperature electronics.

One more important problem to consider, inherent both for SSVs and Josephson MRAM, is the so-called half-select problem [46]. It is the conventionally known RAM scheme: two sets of crossing "word" and "bit" lines, for example along "X" and "Y" directions. The control signal should switch the state of a particular element at the crossing of two lines in a net, whereas the half-amplitude signal should not cause a switch of all other elements along crossing lines. This requirement provides the addressed switch of a particular memory element in RAM. It means that two logical states of a memory element should be separated by a potential barrier. Multilayered structures with continuous magnetization reversals do not solve this problem. In contrast, it has been pointed out [47] that S/M bilayers composed of a spiral magnet M having a potential barrier between two spiral directions due to cubic anisotropy may work both as SSVs and Josephson MRAM. Recently, a new way of control of such SSVs was developed [48], with a nondestructive superconducting state method which is based on magnonic relaxation after a magnetic field pulse. It has been established [48] that the spiral SSVs allowing such a control should have parameters (record-readout speed and stability) comparable with modern MRAM.

In this paper we explore this idea quantitatively [47] where spiral magnets of the B20 family, such as MnSi, (Fe,Co)Si, FeGe, etc., taken in bulk, or etched films, may provide the full T_c switch by a change of the spiral direction. The latter is possible thanks to the cubic noncentrosymmetric magnetic structure of B20 crystal family [49–51] providing asymmetric Dzyaloshinski-Moriya exchange [52]. The magnetic spiral structure, characterized by the spiral vector $\mathbf{Q}$, may be aligned in few equivalent directions under the control of a weak external magnetic field. These preferred directions are determined by the potential barrier that depends on the compound [53]. This provides the above-mentioned advantages for their use as MRAM switchable elements. These magnetic compounds and their films are now in focus

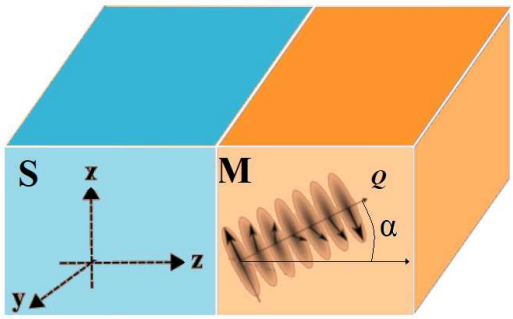

FIG. 1: Sketch of the studied SSV with the spiral wave vector $\mathbf{Q}$ tilted at an angle α to the normal of the S/M interface.

[54, 55] as a medium for magnetic topological defects like skyrmions. Thin films of MnSi, having a strong in-plane magnetic anisotropy, host only a magnetic spiral order with $\mathbf{Q}$ perpendicular to the film plane [56]. The T_c control in superconducting bilayers based on them, may be performed by a reversible uniform magnetization of the films in an external magnetic field. Such elements may be used in biased RAM. Here we theoretically investigate both possibilities of using S/M bilayers as switchable elements for cryogenic electronics applications. We find that the magnitude of δT_c is a non-monotonic function of the spiral wave vector depending on the amplitudes of the exchange field. This behavior can be exploited for the optimization of the structures.

This paper is organized as follows: Sec. II presents the model and the general method for the derivation of T_c in the S/M bilayer, while Sec. III discusses the obtained numerical results for T_c. Sec. IV concludes this work. The details of the analytical calculations are presented in the Appendix.

II. MODEL

To describe the superconducting proximity effect with a spiral magnet, we use linearized Usadel equations in the form [57] valid close to T_c in the dirty limit, usually satisfied in hybrid structures prepared by sputtering. In this limit the superconducting coherence lengths in the M and S layers are given by $\xi_{f,s} = \sqrt{D_{f,s}/2\pi T_{cb}}$, where $D_{f,s}$ are the corresponding electron diffusion coefficients and T_{cb} is the critical temperature of the bulk superconductor.

Here we have developed the calculation method, which allows us to consider limits of both weak and strong exchange splitting h, as well as to examine the behavior at arbitrary value of h (as long as the Usadel equations remain valid) for a long and short spiral period. Moreover, we consider here a finite thickness for the magnetic layer, and the related effects, such as re-entrant super-

conductivity, which also depend on the spiral magnetic order. The third advance of the presented method in comparison with previous theories [47, 57, 59–64] is that it permits the calculation of T_c at arbitrary angles between the spiral wave vector $\mathbf{Q}$ and the S layer plane.

A. Usadel equations for the magnetic spiral inclined for arbitrary angle

We consider a superconducting layer (S) with a finite thickness d_s in proximity with a layer of spiral magnet (M) of thickness d_f. The spiral vector $\mathbf{Q}$, is taken inclined with the angle α with respect to the OZ direction, orthogonal to the layers plane, see Fig. 1. We assume that $\mathbf{Q}$ lies in the XOZ plane, while the XOY plane coincides with the SM interface [65].

The linearized Usadel equations have the general form [57, 58]

$$\begin{aligned}\left(D\nabla^2 - 2\left|\omega\right|\right) f_s &= -2\pi\Delta + 2i\ sgn(\omega)\,\mathbf{h}\cdot\mathbf{f}_t,\\ \left(D\nabla^2 - 2\left|\omega\right|\right)\mathbf{f}_t &= 2i\ sgn(\omega)\,\mathbf{h}\, f_s,\end{aligned} \tag{1}$$

where the singlet f_s and triplet $\mathbf{f}_t = (f_x, f_y, f_z)$ spin components of the anomalous Green's function describe the different superconducting correlations. The singlet superconducting order parameter $\Delta = \Delta(z)$ is nonzero only in the S layer, while the exchange spin splitting $\mathbf{h}(x,z)$ aligned along the local magnetization is nonzero only in the M layer. By taking into account the even symmetry of the singlet components and the odd symmetry of the triplet ones with respect to the Matsubara frequency $\omega \equiv \omega_n = \pi T(2n+1)$ with n a positive or negative integer, we may consider in the following only positive ω.

As a result of the presence of the S/M interface and of the proximity effect, the superconducting correlations naturally depend on the distance to the interface, i.e., they exhibit a z-dependence. For an inclined spiral vector $\mathbf{Q}$, the magnetic vector $\mathbf{h}$ displays an explicit spatial dependence on both variables x and z, so that the problem we consider is in general a two-dimensional one. However, as we show in the Appendix, the extra dependence on x due to the rotating spiral when $\alpha \neq 0$ can be gauged away via a suitable transformation on the triplet vector $\mathbf{f}_t$, so that the original problem is mapped to the following effective one-dimensional one for the new triplet components $f_-(z)$ and $f_+(z)$ in the magnetic layer (see the Appendix for the detail):

$$\begin{aligned}&\left(\frac{\partial^2}{\partial z^2} - \frac{2\omega}{D_f}\right) f_s = i\ \frac{h}{D_f}\left[f_- - f_+\right],\\ &\left[\frac{\partial^2}{\partial z^2} \mp 2iQ\cos\alpha\frac{\partial}{\partial z} - Q^2 - \frac{2\omega}{D_f}\right] f_\pm = \mp 2i\ \frac{h}{D_f} f_s,\end{aligned} \tag{2}$$

with h and Q the amplitudes of the exchange splitting and of the spiral wave vector, respectively. The form of these equations reproduces the limiting cases of the spiral orthogonal and parallel to the interface $\alpha = 0, \pi/2$ which were considered in Refs. 47 and 57. The presence of linear terms in the spiral vector Q reflects the chirality of the spiral, which is related to the broken inversion symmetry of the magnetic lattice that can be found in compounds of the B20 family for instance. The chirality makes the calculations rather more complicated than in the case assuming uniform magnetization.

B. Characteristic equation

If the M layer is semi-infinite and occupies the half-space $z > 0$, the solutions of the linear differential Eqs. (2) take the simple form $f_j(z) = u_j \exp(-k_i z)$, where $j = s, +, -$. Here, we assume the more general situation of a M layer with a finite thickness. This means that we also have to consider spatial solutions with $-k_i$, describing the waves reflected from the free M interface.

The amplitude coefficients for these solutions are determined by the boundary conditions. Here the wave vectors $\pm k_i$ are the eigenvalues of the system (2) and we represent in the following the components of these two related eigenvectors by $u_j,\ v_j$. Let us also introduce the characteristic momenta $k_\omega = \sqrt{2\omega/D_f},\ k_h = \sqrt{h/D_f}$. Eqs. (2) lead to the system of algebraic equations

$$\begin{aligned}\left(k^2 - k_\omega^2\right) f_s - i\ k_h^2 f_- + i\ k_h^2 f_+ &= 0,\\ \pm 2i\ k_h^2 f_s + \left(k^2 - k_\omega^2 \pm 2iQk\cos\alpha - Q^2\right) f_\pm &= 0.\end{aligned} \tag{3}$$

The characteristic equation of this system yielding the eigenvalues k_i is

$$\begin{aligned}\left[(k^2 - k_\omega^2 - Q^2)^2 + 4Q^2k^2\cos^2\alpha\right]\left(k^2 - k_\omega^2\right)&\\ +4k_h^4(k^2 - k_\omega^2 - Q^2) = 0.&\end{aligned} \tag{4}$$

This bicubic equation displays 3 pairs of solutions $\pm k_i$ with Real $k_i > 0$, which are the eigenvalues of the system (2). In the limit $k_h^2 \gg Q^2, k_\omega^2$ the 3 eigenvalues are similar to that found in the orthogonal case: two short-range components $k_\pm \approx (1 \pm i)\, k_h$, and one long-range component $k_0 \approx \sqrt{k_\omega^2 + Q^2}$. Assuming a large exchange energy $h = 100$ meV, one may for instance estimate the quasimomenta as [47] $k_h = \xi_h^{-1} \sim 0.7\,\mathrm{nm}^{-1},\ k_\omega \sim 1/7\,\mathrm{nm}^{-1} = 0.14\,\mathrm{nm}^{-1}$, that yields the inequalities $k_h > Q > k_\omega$. The approximation of strong exchange energy for the values of $k_{\pm,0}$ is thus valid for $h = 100$ meV with an accuracy of two decimal places. But the approximate eigenvectors $(-1,-1,1),\ (1,-1,1)$ and $(0,1,1)$ associated to these eigenvalues have an accuracy of one decimal place only.

Therefore, in the general case we have solved exactly the characteristic equation (4), with the found eigenvectors u_j and v_j written in Appendix. Note that, in the approximation of large exchange splitting, the found eigenvalues and eigenvectors naturally coincide with the ones described previously in the two limiting cases of the spiral parallel to the S/M interface [57, 68] ($\alpha = \pi/2$) and of the spiral orthogonal to the S/M interface ($\alpha = 0$) for semi-infinite [47] and finite [59] M layers.

The solution of the Usadel equations for the finite M layer may finally be found in the general form

$$f_j(z) = \sum_i A_i u_j(k_i) \exp(-k_i z) + B_i v_j(k_i) \exp(k_i z). \quad (5)$$

The coefficients A_i and B_i are then determined from the boundary conditions discussed in the next Section.

C. Boundary conditions

Kupriyanov-Lukichev [69] boundary conditions for the singlet and triplet components of the anomalous Green's function read at the free interfaces

$$\frac{\partial}{\partial z} f_{s,t} = 0, \quad (6)$$

and at the SM interface located at $z = 0$

$$\xi_s \frac{\partial}{\partial z} f^S_{s,t} = \gamma \xi_f \frac{\partial}{\partial z} f_{s,t}, \quad (7)$$
$$f^S_{s,t} = f_{s,t} - \gamma_b \xi_f \frac{\partial}{\partial z} f_{s,t}.$$

Here we have introduced the dimensionless interface parameters $\gamma_b = R_b A \sigma_f / \xi_f$ and $\gamma = (\sigma_f/\sigma_s)(\xi_s/\xi_f)$. The quantities R_b and A are, respectively, the resistance and the area of the S/M interface, and $\sigma_{f,s}$ is the conductivity of the M or S metal. The superscript S in the components f^S_s or f^S_t is used to specify that the correlations are evaluated from the superconducting side, while the absence of superscript holds for the magnetic side.

Since the Usadel equations have been rewritten in terms of the transformed triplet components $f_\pm(z)$, we need to derive the boundary conditions for these functions instead. As shown in Appendix, we get the boundary conditions for the free interfaces at $z = d_f$ and $z = -d_s$ for the inclined case corresponding to the linearized Usadel equations (2)

$$\frac{\partial}{\partial z} f_s(d_f) = 0, \qquad \frac{\partial}{\partial z} f_\pm(d_f) = \pm iQ \cos\alpha \, f_\pm(d_f), \quad (8)$$
$$\frac{\partial}{\partial z} f^S_{s,\pm}(-d_s) = 0,$$

and the boundary conditions at the S/M interface at $z = 0$

$$\xi_s \frac{\partial}{\partial z} f^S_s(0) = \gamma \xi_f \frac{\partial}{\partial z} f_s(0),$$
$$\xi_s \frac{\partial}{\partial z} f^S_\pm(0) = \gamma \xi_f \left(\frac{\partial}{\partial z} \mp iQ \cos\alpha \right) f_\pm(0), \quad (9)$$
$$f^S_s(0) = f_s(0) - \gamma_b \xi_f \frac{\partial}{\partial z} f_s(0),$$
$$f^S_\pm(0) = f_\pm(0) - \gamma_b \xi_f \left(\frac{\partial}{\partial z} \mp iQ \cos\alpha \right) f_\pm(0).$$

The sign $\pm$ in front of the contributions depending on Q expresses the chirality of the magnetic spiral: clockwise or anticlockwise. In the presence of a finite thickness for the magnet, this chirality leads to a calculation complexity, which was not taken into account by previous works. Note, however, that the superconducting critical temperature turns out to be independent of the chirality sign owing to the spin symmetry of the superconducting wave function in S.

D. Critical temperature calculation

The singlet component $f^S_s(z)$ in the superconductor depends on the superconducting gap $\Delta(z)$, which is calculated self-consistently. The required closed boundary value problem for the singlet component f^S_s includes the Usadel equation (2) in the superconducting layer, and the boundary condition in the form

$$\xi_s \frac{\partial}{\partial z} f^S_s \Big|_{z=0} = - W f^S_s|_{z=0}. \quad (10)$$

The real-valued quantity W contains the entire information about the proximity effect with the spiral magnet, and may be written as

$$W = \gamma \left[\frac{\sum_i S_i u_s(k_i)}{\xi_f \sum_i R_i k_i u_s(k_i)} + \gamma_b \right]^{-1}, \quad (11)$$

with the coefficients R_i and S_i defined in the Appendix.

Finally, we compute numerically the critical temperature T_c of the superconducting layer, via the use of the self-consistent equation

$$\ln \frac{T_{cb}}{T_c} = \pi T_c \sum_{\omega=-\infty}^{\infty} \left(\frac{1}{|\omega|} - \frac{f^S_s(z)}{\pi \Delta(z)} \right) \quad (12)$$

by using the method of fundamental solution [57, 70, 71].

E. Model parameters

For the realization of the presently studied SSV, different types of spiral magnets may be considered, thus providing various possible ranges of values for the model parameters. Of course, this variety can be exploited to optimize the switching control and the spin-valve behavior in the S/M bilayer. In this section, we address in some detail the possibilities so far available nowadays from real materials and the associated variable ranges, such as for example for the magnitudes of the exchange splitting h or for the spiral wave vector Q.

Metals of the B20 family like MnSi, (Fe,Co)Si, FeGe, etc., are arranged in a crystal lattice of cubic symmetry with broken inversion symmetry. The latter provides an asymmetric Dzyaloshinsky-Moriya exchange leading to the spiral magnetic order. For Lanthanide metals like Ho or Er, the spiral magnetic order stems from the competitive magnetic exchange of close neighbours and next

neighbours. Although having a different microscopic nature, at the level of the proximity effect these magnetic materials exhibit similar properties when described in the mean field approximation.

On account of the lattice symmetry in B20 materials the magnetic spiral characterized by the vector **Q** may align in few different directions in the ground state (in the absence of an external magnetic field). Depending on the compound, the preferred spiral directions may be along the cubic axes [100], [010], [001] for FeCoSi and MnGe, and along the diagonals of the cube $[1 \pm 1 \pm 1]$ for MnSi. Depending on the magnetic history [53] the spiral may even have an arbitrary direction at a weak cubic anisotropy as for example in FeCoSi. The direction of **Q** may be controlled by a relatively weak external magnetic field of the order of 100 Oe for MnSi. It is important for the applications in SSVs to have the control field lower than the critical magnetic field of superconducting films, which is $\sim$ 30 kOe for the in-plane direction of the Nb superconductor. Very recently, a method to control a bilayer SSV which does not perturb its superconducting state has been proposed and optimized [48] via numerical experiments on the MnSi/Nb bilayer SSV. A switching between few ground state magnetic configurations (separated by a potential barrier) with different directions of the magnetic spiral **Q** is found to be carried out by a several hundred ps in duration magnetic field pulse of several kOe in magnitude. Such a pulse does not destroy the superconducting state of the Nb layer by itself but leads to the excitation of magnons in the magnetic layer, which trigger the reorientation process of the magnetic spiral [48]. The system can be switched there and back by magnetic fields of opposite signs along one direction in the layers plane, thus permitting an easy control. The switching time is estimated [48] as several nanoseconds, which coincides with the scales of the spin-transfer torque MRAM recording time making this method attractive for energy saving cryogenic electronics.

The absolute value of the spiral vector is defined as $Q = 2\pi/\lambda$, where λ is the spiral spatial period. The spiral antiferromagnets of the B20 family may have short or long spiral spatial periods (from 3 nm for MnGe up to 90 nm for Fe(0.5)Co(0.5)Si) that reflect the relation between the Dzyaloshinsky-Moriya interaction and the exchange energy. In the spiral magnetic metal MnSi with $\lambda = 18$ nm the preferred spiral directions $[1 \pm 1 \pm 1]$ have the angle $\arccos(1/3) = 70.5°$. If two of these directions lie in the film plane, the other two have the angle $\alpha = \pi/2 - \arccos(1/3) = 19.5°$ with the normal OZ to the interface. In this case the structure is periodic in OX direction with the large period $\lambda/\sin\alpha = 54$ nm, which is much larger than other characteristic lengths such as $\lambda/2\pi$ or the superconducting coherence length ξ_f. The period of the spiral in OZ direction increases only slightly, since $\lambda/\cos\alpha = 19$ nm.

Recently, there have been some evidence that MnSi has a relatively weak exchange splitting [72, 73]. In the compound MnSi, the amplitude of the exchange field has even been estimated [73] to the relatively low value $h = 11$ meV. We could take the estimated value of the exchange as an upper limit for the exchange splitting of the superconducting electrons in the mean field approximation. However, the exchange splitting magnitude may be larger for other compounds of the B20 family. The Curie temperature may work as a signature of the exchange energy magnitude, though without direct proportionality. It varies from about 29 K for MnSi to 279 K for FeGe. Thus, the Curie temperature is larger than the T_c of s-wave BCS superconducting metals like Al or Nb usually used in cryogenic nanotechnology.

As a result of the asymmetric exchange interaction, topological magnetic defects called skyrmions exist in such compounds at high magnetic fields and at temperatures close but lower than the Curie temperature [74, 75]. These defects carry nontrivial topological charge. Because of possible applications in spintronics [76], as well as of the fundamental interest for physical properties dictated by topology, these compounds and their films are now under very intensive theoretical and experimental investigations. There exists an experimental method to prepare films of B20 compounds from the single crystals by etching [77–79]. Such films have the same magnetic properties as bulk crystals, albeit with lower thicknesses. Seemingly, thin films of MnSi grown by molecular beam epitaxy (MBE) or by electron beam lithography often do not host skyrmions, presumably due to their high in-plane magnetic anisotropy. In these structures, the magnetic spiral may align only with **Q** orthogonal to the film plane. At $d_f < \lambda$ the incomplete period of the magnetic spiral may be continuously collapsed towards the uniform magnetization replacing the conical phase in a parallel magnetic field about few kOe up to around 1.3 T for MnSi. This effect may be also used to tune T_c in the S/M bilayer, by gradually destroying the LRTC when approaching the uniform magnetization situation.

In contrast, the spiral magnetic order in lanthanide 4f metals, like Ho or Er which have been widely used in experiments on the superconducting proximity effect, is characterized by a short spiral period of about 4 nm for Er and 6 nm for Ho, and probably by a large exchange splitting. Furthermore, the magnetic anisotropy of such lanthanide films is usually strongly in-plane.

Other model parameters. For the T_c calculations, the superconducting layer is assumed to be made of Nb, with the superconducting coherence length $\xi_s = 11$ nm. The critical temperature of the bulk superconductor is taken as $T_{cb} = 9.2$ K. The superconducting coherence length in the M layer is chosen to be $\xi_f = 4.2$ nm. The S/M interface transparency is taken from the realistic estimations made in Ref. 80 with $\gamma_B = 0.7$, and the interface parameter [47] is chosen as $\gamma = 0.7$.

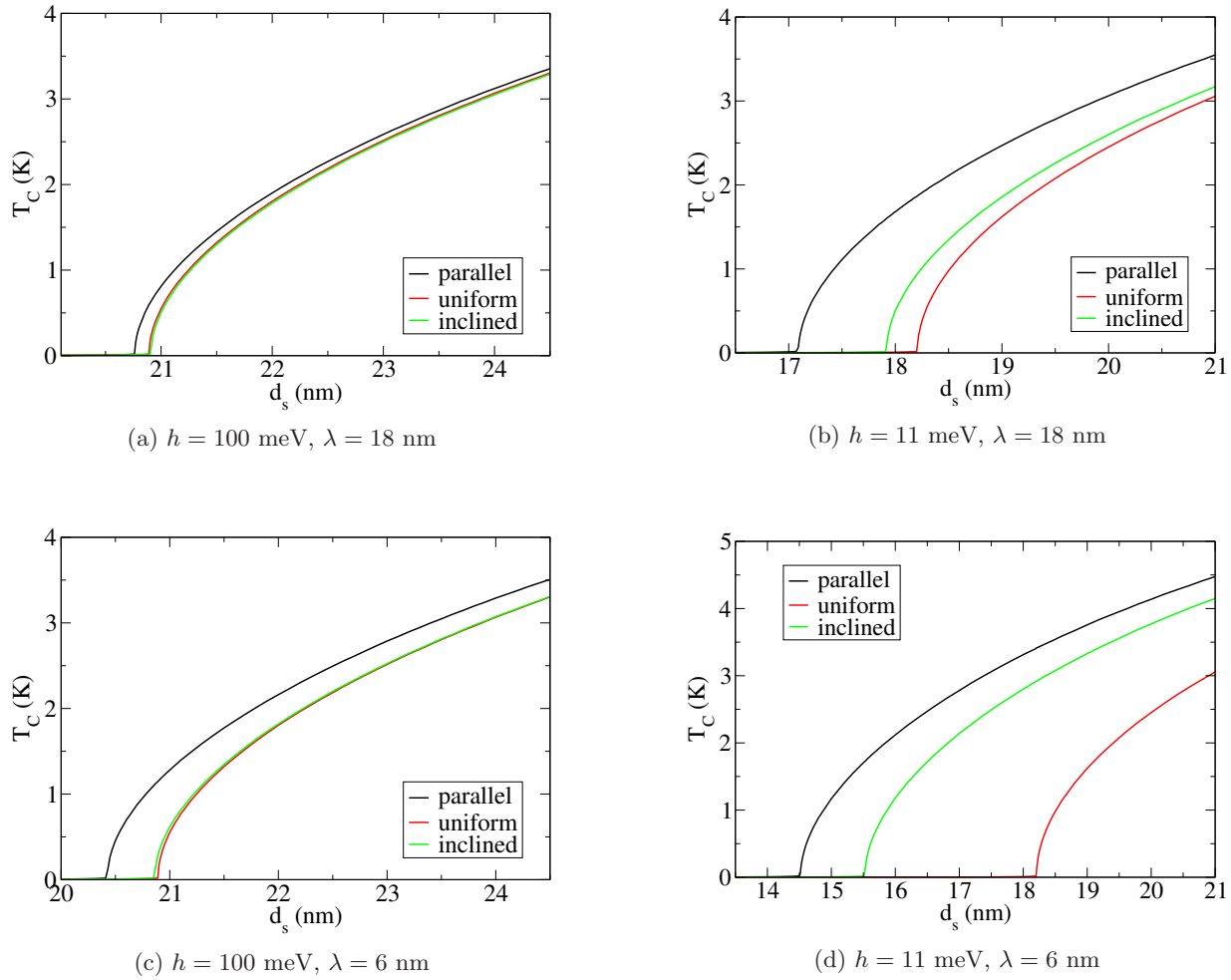

(a) $h = 100$ meV, $\lambda = 18$ nm

(b) $h = 11$ meV, $\lambda = 18$ nm

(c) $h = 100$ meV, $\lambda = 6$ nm

(d) $h = 11$ meV, $\lambda = 6$ nm

FIG. 2: Superconducting critical temperature T_c as a function of the S layer thickness d_s within three different magnetic configurations. The different panels (a), (b), (c), (d) correspond to different values of the exchange energy and spiral period. The large and small exchange field cases are characterized by the typical values $h = 100$ meV and $h = 11$ meV, respectively. The long and short spiral period situations correspond to $\lambda = 18$ nm and $\lambda = 6$ nm, respectively.

III. RESULTS AND DISCUSSION

The superconducting critical temperature T_c of the S/M bilayer has been systematically studied and compared in the three configurations of a spiral parallel to the S/M interface ($\cos\alpha = 0$), of a spiral inclined to the interface normal by the angle $\alpha = 19.5°$ (i.e., $\cos\alpha \approx 0.94$), and of a uniform magnetization (in this case, the superconducting properties are independent of the angle α and $Q = 0$). These three configurations permit the comparison between two possible switching behaviors of the SSV, which may be considered experimentally. If the S film is covered by a bulk or etched crystal of a spiral magnet of the B20 family, the change of T_c may be achieved by the switch between parallel and inclined (maybe perpendicular) spiral. Alternatively, in the case of the proximity with a M film characterized by a strong in-plane magnetic anisotropy (as in Ho, Er, or thin B20 family films), for which the spiral vector is always perpendicular to the film plane, the T_c switch may be realized by the collapse to the uniform magnetization.

In Figs. 2, the dependencies of T_c on the superconductor thickness d_s are first analyzed for different spiral configurations. Fig. 2a shows that, at a strong exchange field, the critical temperature T_c for a parallel spiral is larger than that obtained for a uniform magnetization. This can be easily understood by the effective space averaging of the exchange field at the Cooper pair size scale. In contrast, for the inclined spiral, T_c is (slightly) reduced in comparison to the uniform case because of the draining of the Cooper pairs from the S layer into the open long-range triplet channel. This figure illustrates that the S/M proximity effect is driven by two competing mechanisms which affect the value of T_c: i) an effective space averaging of the exchange field (mostly governed by the wave vector Q of the spiral), and ii) the appearance of the

LRTC (controlled by the spiral angle and the exchange amplitude) which tends to suppress T_c.

In fact, the relative role of these two mechanisms depends on the relation between all characteristic wave vectors (e.g., including the exchange quasi-momentum k_h defined from the exchange energy h, and the superconductor quasi-momenta related to the coherence lengths in the S and M layers), so that the resulting behavior for T_c turns out to be a many-parametric problem. Thereby, it is revealed in Fig. 2b that the consideration of a smaller value for the exchange field h than in Fig. 2a can implement an opposite order for the T_c values, since the T_c for an inclined spiral is now larger than in the uniform case. It can also be seen in Fig. 2b that the spin-valve effect for the set of parameters related to MnSi [73] may become giant achieving a $\delta T_c \sim 1.6 - 1.8$ K depending on the switch to the inclined spiral or uniform magnetization. An even larger spin-valve effect is displayed in Fig. 2d where both a low exchange field and a short spiral period are considered. This case reveals the search direction for a suitable magnetic compound leading to the largest spin-valve effect. As expected, the strongest effects resulting from the S/F interplay may be found in the regime where all characteristic lengthscales (the S and F superconducting coherence lengths, the spiral wavelength λ, and the magnetic length $\xi_h = k_h^{-1}$) are of the same order.

To understand the behavior according to the two highlighted mechanisms i) and ii), it is important to remind that the long-range and short-range triplet superconducting correlations are characterized by quite different dependencies on the exchange field, which are best discriminated at strong fields: the former has a h-independent coherence length $\sim (k_\omega^2 + Q^2)^{-1/2}$, while the latter can be associated to the lengthscale $\sim (k_\omega^2 + k_h^2)^{-1/2}$, which is roughly inversely proportional to $\sqrt{h}$. The physical reason for this discrepancy is that the LRTC are not subjected to the depairing influence of the exchange field, so that both electrons in the Cooper pair can have the same spin projection to the field direction. Therefore, an increasing exchange field favors the draining of the Cooper pairs into the LRTC channel rather than into the short range triplet channel with $S_z = 0$. At low fields, the LRTC appear as a correction effect in comparison with the predominantly generated short-range correlations, and thus hardly affect the superconducting properties of the M/S bilayer. In the low-exchange field regime, the T_c dependence on the spiral direction is mainly determined by the averaging mechanism: when the direction of the penetration of the Cooper pairs into the magnet does not coincide with the direction of averaging, this averaging becomes more effective, and then, T_c proved to be less suppressed, cf. Fig. 2b.

Interestingly, this averaging effect on T_c may be even more pronounced in magnitude than that accompanied by the LRTC creation. It has already been noticed [81] that the scale of space modulation of superconducting properties in the junction plane may differ from the one out of plane. In the present study, one can also see the similarity between the integral energetic characteristics like T_c and the Josephson current. In the case of T_c, the out-of-plane modulation scale is weakened due to the competition with the proximity effect leakage mechanism occuring in the same direction, so that out-of-plane modulations play quantitatively a minor role than the in-plane ones. If one ignores the LRTC, one can understand this effect in the following way. For a perpendicular or slightly inclined spiral, the Cooper pairs encounter, when penetrating into the M layer, an almost uniform exchange field and feel its modulations weakly as they propagate. On the contrary, for a magnetic spiral parallel to the interface, they experience an exchange field averaged out over the full Cooper pair size extension.

As already remarked above, the low exchange field value in the compound MnSi yields, *a priori*, an important spin-valve effect. As is clear from the previous discussion, another way to enhance the switching effect is to prefer magnetic materials with strong spatial modulations, as the mean exchange averaging becomes more effective for a short spiral period. This situation is encountered, e.g., in Ho with the relatively short spiral period $\lambda = 6$ nm. The corresponding T_c dependencies for the different spiral configurations are displayed in Fig. 2c (we have chosen here $h = 100$ meV because we believe that pure 4f metals still have strong exchange).

From now on, we will consider a S/M bilayer with a fixed S thickness ($d_s = 21$ nm; this value is chosen as more or less optimal to exhibit the dependencies) and analyze the T_c variations with respect to various other model parameters. We show in Fig. 3 that the interplay between the averaging and the LRTC mechanisms is also exhibited in the dependence of the superconducting critical T_c on the spiral wave vector $Q = 2\pi/\lambda$. For a large exchange field, we clearly see in Fig. 3a an extremum in the T_c dependence of the inclined spiral. It is the result of the competition between the T_c suppression by the LRTC, which is more important at a long spiral, i.e., at small Q, and the effective averaging mechanism, which leads to the growth of T_c at a short spiral period, i.e., at large Q. Note that this competition does not occur in the case of a spiral parallel to the interface, for which the LRTC is absent: T_c displays a monotonic increase as a function of Q due to the more efficient averaging effect when reducing the characteristic spatial modulation of the exchange field. In contrast, at a smaller exchange field, the LRTC creation mechanism becomes less relevant, so that the extremum for the inclined configuration is shifted to much smaller values of Q as revealed in Fig. 3b. In this situation the averaging effect wins for most spiral periods.

To make clear the role of the exchange energy in the interplay of the two underlined mechanisms governing the T_c behavior, we also present in Fig. 4a the dependence of T_c on h for a long spiral period (case of MnSi with $\lambda = 18$ nm). It is seen that the T_c in the different configurations display a similar (roughly parallel) decreasing

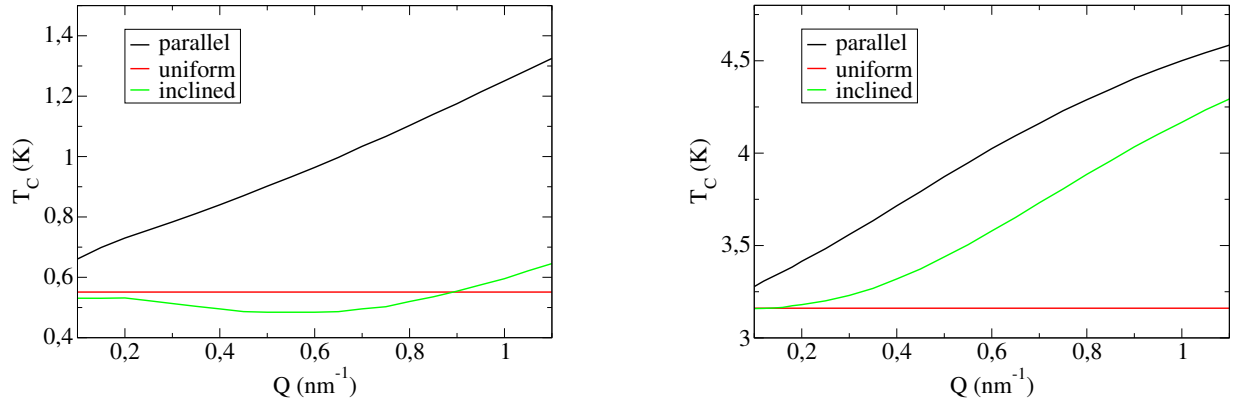

(a) $h = 100$ meV (b) $h = 11$ meV

FIG. 3: Superconducting critical temperature T_c as a function of the spiral wave vector Q within three different magnetic configurations, for (a) large and (b) small exchange energy h (i.e., $h = 100$ meV and $h = 11$ meV, respectively). Here, we consider the layer thicknesses $d_f = 40$ nm and $d_s = 21$ nm.

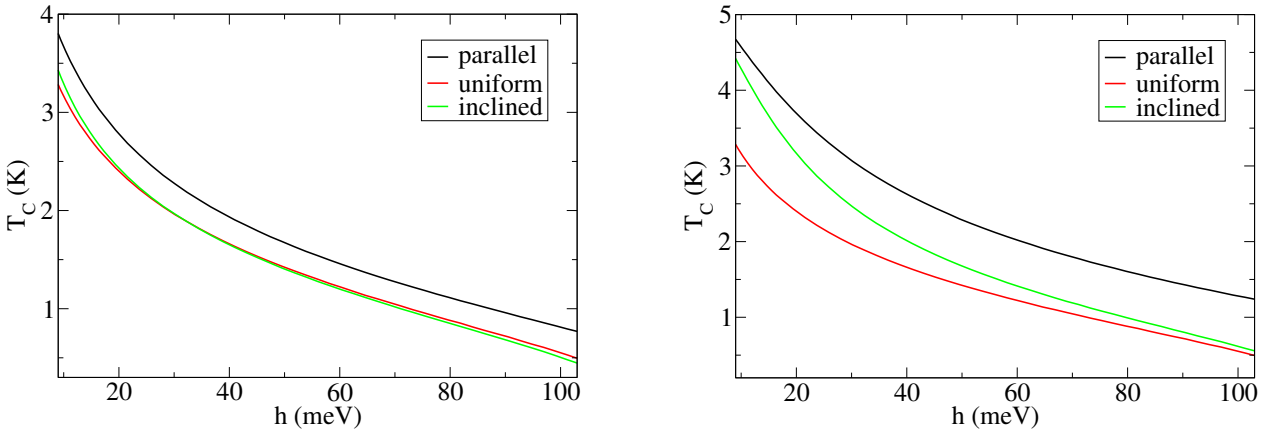

(a) $\lambda = 18$ nm (b) $\lambda = 6$ nm

FIG. 4: Superconducting critical temperature T_c as a function of the exchange energy h within three different magnetic configurations, (a) for large spiral spatial period $\lambda = 18$ nm (as in MnSi), and (b) for short spiral spatial period $\lambda = 6$ nm (as in Ho). We have taken $d_s = 21$ nm and a large M layer thickness $d_f = 40$ nm$\gg \xi_f$.

tendency. In the low exchange field regime, the inclined case provides a slightly higher T_c than in the uniform case, whereas at higher exchange values it yields a lower T_c. In the inclined spiral configuration, the growth of h entails an increasing role of the LRTC in the proximity effect, which efficiently weaken superconductivity of the S layer. At a smaller spiral period as in Ho ($\lambda = 6$ nm), the difference in the $T_c(h)$ behavior between the uniform and inclined configurations is more pronounced, see Fig. 4b. The lowest T_c is then always obtained in the uniform case.

The finite thickness of the M layer taken into account in our model calculations allows us to consider the phenomenon of reentrant superconductivity according to the spiral configuration, which is studied in some detail in Figs. 5. It is pointed out that if one magnetic configuration provides the reentrant behavior, i.e., $T_c = 0$ in some range of thicknesses d_f, the full switch of superconductivity may then be achieved in this range with the change of the magnetic configuration. With the decrease of the magnetic exchange energy (compare Fig. 5a and Figs. 5b, 5c) the period of the T_c oscillation becomes larger, as one could expect. It thus creates better conditions for the experimental implementation of such reentrant behavior, by providing wider regions of d_f where $T_c = 0$ for a given magnetic configuration and nonzero T_c (in the Kelvin range) for another magnetic configuration. Note that the nature of the magnetic configuration yielding a vanishing T_c in a given d_f range also depends on the magnetic exchange amplitude, in accordance with Figs. 4. For thin films grown with a strong in-plane anisotropy a possible switch may be realized by commut-

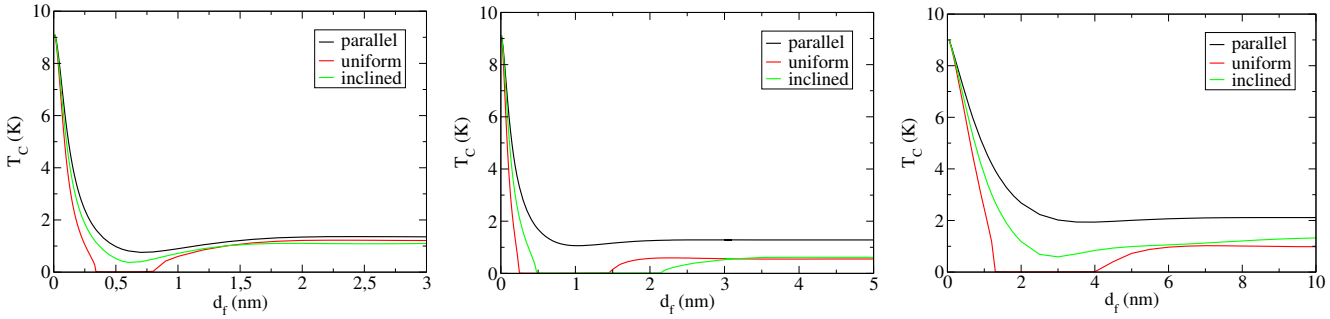

(a) $h = 100$ meV, $\lambda = 18$ nm (b) $h = 100$ meV, $\lambda = 6$ nm (c) $h = 11$ meV, $\lambda = 18$ nm

FIG. 5: Superconducting critical temperature T_c as a function of the M layer thickness d_f within within three different magnetic configurations, (a) for large exchange energy $h = 100$ meV, large spiral spatial period $\lambda = 18$ nm and $d_s = 21.4$ nm, (b) large exchange energy $h = 100$ meV, short spiral spatial period $\lambda = 6$ nm and $d_s = 21$ nm (Ho case), and (c) for small exchange energy $h = 11$ meV, large spiral spatial period $\lambda = 18$ nm and $d_s = 18.5$ nm (MnSi case).

ing the magnetic system from a spiral perpendicular to the layer to a uniform magnetization configuration, which may be achieved for a thickness smaller than the spiral period under the application of a relatively small magnetic field. From this analysis, one may conclude that the compounds of the B20 family seem preferable for the observation of the controlled reentrant superconductivity phenomenon and for the realization of the full switch of T_c to zero.

Finally, our model calculations also allow us to study the T_c dependence on the angle α between the spiral vector $\mathbf{Q}$ and the S/M interface normal, see Figs. 6 with two different sets of parameters, one suitable for MnSi (Fig. 6b) and the other one for Ho (Fig. 6a). In the two cases, the same general trend is found, namely the monotonic growth of T_c with the angle α, with an initial T_c lower than the T_c obtained in the uniform magnetization case. This stronger suppression of superconductivity for a spiral perpendicular to the film is due to the presence of the LRTC, whose generation is controlled by the angle (with a maximal production for $\alpha = 0$). The comparison between Fig. 6a and Fig. 6b shows that the LRTC plays a role at lower exchange field and at larger spiral period only within a small range of angles α for which we encounter the unusual situation where an applied magnetic field magnetizing the film uniformly may lead to an increase of the T_c of the bilayer.

IV. CONCLUSION

To summarize, we have studied in detail a superconducting spin valve consisting of a superconducting film covered by a spiral magnet characterized by multiple equilibrium configurations. We have considered spiral magnets of different types: Ho and Er, or B20 family compounds, both crystals and films. These SSVs may be controlled by biased or pulse external magnetic field, producing magnetization reversal or magnonic relaxation resulting in the magnetic spiral reorientation. They present not only a fundamental theoretical interest, but also a technological one, as exemplified by earlier experimental works [44, 45] on Er or Ho bilayers and recent experimental efforts to create MnSi based SSVs [82].

In comparison with the theoretical work developed previously in Ref. 47 and 59 on the same model, we have presented here an extended derivation including a few significant improvements: i) an arbitrary value of the exchange energy, suitable for MnSi for example, is considered, whereas a large value was assumed previously [47]; ii) the magnetic spiral vector can be inclined at an arbitrary angle with respect to the interface (for simplicity, only parallel and perpendicular spirals were considered in Ref. 47); iii) the finite thickness of the magnetic layer is taken into account, in contrast to the previous work [47] assuming a semi-infinite M layer.

Besides providing a more realistic description of the possible experimental conditions and justifying some simplifications made in the previous work, this enlargement of the parameter space reveals quite different qualitative behaviors for the spin valve depending on the spiral configuration. In particular, we have found that the superconducting critical temperature may significantly vary as a function of the spiral direction also at moderate or low exchange energies. In this parameter regime, the superconducting correlations resulting from the proximity effect between the superconducting film and the chiral magnet are primarily short-range, so that the sensitivity of T_c is only due to the averaging of the exchange field on the scale of the Cooper pairs. It turns out that this averaging effect is much more efficient when the direction of the penetration of the Cooper pairs (which is perpendicular to the interface) does not coincide with the direction of the magnetic spatial inhomogeneity. As a result, the parallel spiral configuration always yields the highest T_c, as confirmed by our numerical calculations.

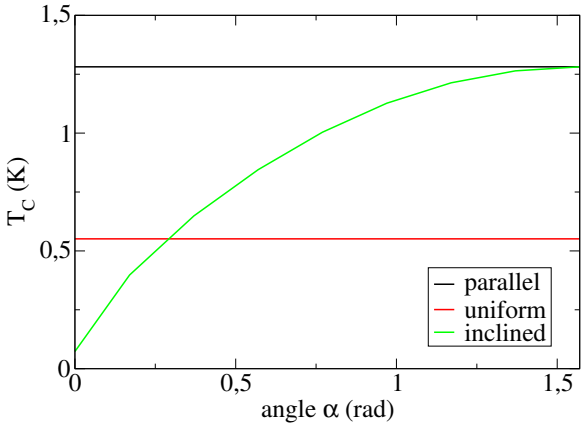

(a) $h = 100$ meV, $\lambda = 6$ nm

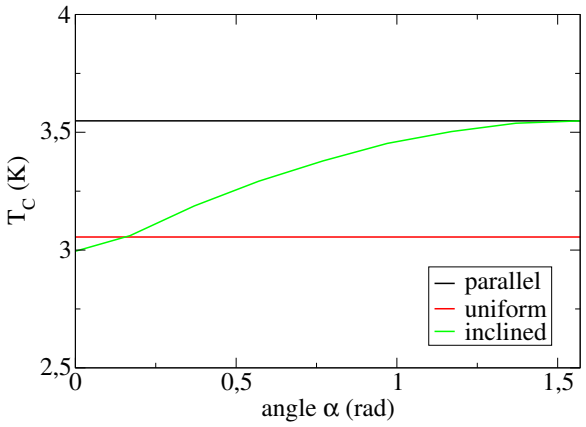

(b) $h = 11$ meV, $\lambda = 18$ nm

FIG. 6: Superconducting critical temperature T_c as a function of the angle α between the spiral vector Q and the S layer normal within three different magnetic configurations, (a) for large exchange $h = 100$ meV and short spiral spatial period $\lambda = 6$ nm (as in Ho), and (b) for small exchange $h = 11$ meV and long spiral spatial period $\lambda = 18$ nm (as in MnSi). We have taken equal layers thicknesses $d_s = d_f = 21$ nm. The curves in the uniform and parallel cases are kept here as reference lines.

In contrast, for large exchange energies a different mechanism of sensitivity of T_c is at play: for a spiral direction orthogonal to the interface the production of long-range superconducting triplet correlations opens a new channel for the leakage of the Cooper pairs from the superconducting film, thus leading to an efficient decrease of T_c. Therefore, the behavior of the studied superconducting spin valve is driven by two different antagonistic mechanisms. Our quantitative analysis of the reentrant superconductivity phenomenon in the bilayer suggests the switching behavior of the superconducting spin valve to be more optimal at moderately low exchange energies, where the averaging mechanism takes over the long-range triplet correlations mechanism.

The most interesting result, which will stimulate further experimental investigation, optimization, and manufacturing of such structures, is that the spin valve effect may yield a δT_c within the Kelvin range in MnSi-Nb bilayers, i.e., may be giant. Therefore, it seems generally preferable to manufacture SSVs with MnSi crystal-Nb bilayers, which furthermore permit nonperturbative magnonic control. The intrinsic solution of the half-select problem and the possibility of magnonic control (nondestructive for superconductivity) make such spin valves appealing for applications in cryogenic nanoelectronics, merging superconducting spintronics and magnonics.

A. Acknowledgements

N.P. thanks D. Menzel, V. Dyadkin, and A. Bauer for helpful discussions about the B20 family properties. The French-Russian collaboration has benefited from the Visiting Scientist Program of the Centre de Physique Théorique de Grenoble-Alpes, and from the invited researcher program of CNRS. The analysis of B20 family based SSVs was financially supported by the Ministry of Science and Higher Education of the Russian Federation, Megagrant project N 075-15-2019-1934. N.P. thanks also the Project Mirror Labs of the HSE University for the support of the analysis of 4f metals - superconductor bilayers. The development of the program for the numerical calculation of T_c was supported by RFBR, project N19-02-00316.

APPENDIX

In this Appendix, we present the detailed derivation of the key-quantity W [see Eq. (11)], which determines the dependences of the superconducting critical temperature on the different model parameters.

For an inclined spiral, the magnetic structure is nonuniform both in OZ and OX directions, so that the different superconducting correlations components in the linearized Usadel Eqs. (1) are expected to be in general functions of both x and z spatial variables, and the Laplacian operator reads $\nabla^2 = \frac{\partial^2}{\partial x^2} + \frac{\partial^2}{\partial z^2}$.

In the orthogonal case ($\alpha = 0$), the spiral vector $\mathbf{Q}$ lies in the OZ direction, and the magnetic field direction is described by the rotation matrix M_z around OZ axis with the rotation phase $\beta = Qz$: $\mathbf{h} = h(\cos\beta, \sin\beta, 0)^T = M_z\,(h, 0, 0)^T$. The linearized Usadel equations take the form in this case:

$$\begin{aligned}
\left(D\nabla^2 - 2\,|\omega|\right) f_s &= 2i\ sgn(\omega) h \left[f_x \cos(Qz) + f_y \sin(Qz)\right], \\
\left(D\nabla^2 - 2\,|\omega|\right) f_x &= 2i\ sgn(\omega) h f_s \cos(Qz), \\
\left(D\nabla^2 - 2\,|\omega|\right) f_y &= 2i\ sgn(\omega) h f_s \sin(Qz).
\end{aligned} \tag{13}$$

From now on, we assume that the axis of the spiral is

inclined in the XOZ plane. This inclined configuration may be obtained from the orthogonal case with the help of the rotation matrix around the OY axis by the angle α (OZ axis rotates towards OX axis by the angle α)

$$M_z = \begin{pmatrix} \cos\beta & -\sin\beta & 0 \\ \sin\beta & \cos\beta & 0 \\ 0 & 0 & 1 \end{pmatrix}, \; M_y = \begin{pmatrix} \cos\alpha & 0 & -\sin\alpha \\ 0 & 1 & 0 \\ \sin\alpha & 0 & \cos\alpha \end{pmatrix} \tag{14}$$

where the inclined spiral vector is given by $\mathbf{Q} = M_y(0,0,Q)^T$. The phase of the exchange field vector rotation around the spiral vector is then $\beta = \beta(x,z) = Q\,(-x\sin\alpha + z\cos\alpha)$. The exchange field vector reads $\mathbf{h} = M_y M_z\,(h,0,0)^T = h(\cos\alpha\cos\beta,\ \sin\beta,\ \sin\alpha\cos\beta)^T$.

The unitary transformation of the triplet components vector $\mathbf{f}_t = (f_x,\ f_y,\ f_z)^T$ to the vector $\mathbf{f}_{pm} = (f_+,\ f_-,\ f_z)^T$ in the orthogonal case ($\alpha = 0$) is given by $\mathbf{f}_{pm} = N\mathbf{f}_t$ with the matrix N

$$N = \begin{pmatrix} -\exp(i\beta) & i\exp(i\beta) & 0 \\ \exp(-i\beta) & i\exp(-i\beta) & 0 \\ 0 & 0 & 1 \end{pmatrix}. \tag{15}$$

In the inclined case ($\alpha \neq 0$) all components of $\mathbf{f}_t$ are nonzero in general. We may then introduce the vector $\mathbf{f}_{pm} = (f_+,\ f_-,\ f_{zz})^T$ given by the linear transformation $\mathbf{f}_{pm} = NM_y^{-1}\mathbf{f}_t$, which transforms the linearized Usadel Eqs. (13) to their linear combination. The equation for the third triplet component f_{zz} separates after the transformation and we may choose $f_{zz} = 0$, that yields the additional condition $f_z = f_x \tan\alpha$.

The explicit dependence on the x variable has completely disappeared in the equations obeyed by the correlation functions $f_{s,\pm}(x,z)$. It can be shown that the latter functions are in fact independent of x. For this purpose, we follow the method of Ref. 57 by expanding the correlations as Fourier series, assuming that the system is periodic in the OX direction: $f_{s,\pm}(x,z) \to f_{s,\pm}(m,z)$ where m is an integer number. Since the equations are linear, the different Fourier components m are fully decoupled. The most energetically favorable solution corresponds [57] to the uniform one with $m = 0$. The other solutions with $m = \pm 1, \pm 2...$ describe the cases of a superconducting order parameter which is spatially inhomogeneous even deeply in the S region and are not realized physically. Finally, we get that the functions $f_{s,\pm}(x,z)$ obey the Eqs. (2) in the ferromagnet, which have a form similar to the orthogonal case with the spiral vector Q being replaced by $Q\cos\alpha$ in the linear term.

The eigenvectors of the system (2) may be chosen for the eigenvalues $k_i = k_{0,\pm}$ as

$$\begin{pmatrix} u_s(k_i) \\ u_-(k_i) \\ u_+(k_i) \end{pmatrix} = \begin{pmatrix} i\frac{k_i^2 - k_\omega^2 + 2iQk_i\cos\alpha - Q^2}{2k_h^2} \\ -\frac{k_i^2 - k_\omega^2 + 2iQk_i\cos\alpha - Q^2}{k_i^2 - k_\omega^2 - 2iQk_i\cos\alpha - Q^2} \\ 1 \end{pmatrix}. \tag{16}$$

For a finite F layer we also have to take into account the wave reflected from the free M layer interface solutions $\sim \exp(k_i z)$. The eigenvectors v_j representing this reflected wave may be obtained with the change $k_i \to -k_i$, considering that only the relation between the eigenvector components has a meaning

$$\begin{pmatrix} v_s(k_i) \\ v_-(k_i) \\ v_+(k_i) \end{pmatrix} = \begin{pmatrix} i\frac{k_i^2 - k_\omega^2 + 2iQk_i\cos\alpha - Q^2}{2k_h^2} \\ -1 \\ \frac{k_i^2 - k_\omega^2 + 2iQk_i\cos\alpha - Q^2}{k_i^2 - k_\omega^2 - 2iQk_i\cos\alpha - Q^2} \end{pmatrix} = \begin{pmatrix} u_s(k_i) \\ -u_+(k_i) \\ -u_-(k_i) \end{pmatrix}. \tag{17}$$

Note that for $\cos\alpha = 0$ (spiral parallel to the SM interface) the two functions $f_\pm$ are identical, thus indicating that only one type of triplet component (of short-range nature) is in fact produced [57] in the hybrid structure in this special configuration. In the inclined case, the system resolution necessarily involves the two different components f_+ and f_- hinting at the coexistence of two types of triplet correlations in the structure. Owing to the chirality, the short-range components (depending on the exchange field h) of the eigenvectors for the incident $\mathbf{u}$ and reflected $\mathbf{v}$ waves display a complicated symmetry $v_\pm = -u_\mp$ including the chirality change ("+" to "-", and opposite). The reflected wave moves along the spiral backward and feels the opposite direction (clockwise or anticlockwise) of the magnetization rotation along the movement direction. It is worth stressing that the combination of chirality and finite thickness for the magnet leads to a computation complexity related to the doubling of the needed coefficient amplitudes, which was actually absent in the previous works [47, 57, 59–64].

The general form of the solution for the finite F layer is written down in Eq. (5). Let us denote $R_i \equiv A_i - B_i$ and $S_i \equiv A_i + B_i$. From the boundary conditions (8) at $z = d_f$, it follows the equations

$$\begin{aligned} &\sum_i \left[R_i \cosh(k_i d_f) - S_i \sinh(k_i d_f)\right] U_{s,-}(k_i) = 0, \\ &\sum_i \left[S_i \cosh(k_i d_f) - R_i \sinh(k_i d_f)\right] U_+(k_i) = 0, \end{aligned} \tag{18}$$

where we have introduced $U_s(k_i) = u_s(k_i)k_i$ and

$$\begin{aligned} U_\pm(k_i) &= V_\pm(k_i)k_i + iQ\cos\alpha V_\mp(k_i). \\ V_\pm(k_i) &= u_+(k_i) \pm u_-(k_i), \end{aligned} \tag{19}$$

In the S layer the spatial non-uniformity is only provided by the nonuniform magnetization existing along the SM interface. It thus seems to be natural to use $\beta = \beta(x,0)$ inside the S region. So the transformation to apply on the different superconducting components has the form $\mathbf{f}_{pm}^S = N(\beta(x,0))M_y^{-1}\mathbf{f}_t^S$, that yields the Usadel equations in the S region

$$\begin{aligned} &\left(\nabla^2 - \frac{2\omega}{D_s}\right) f_s^S = -2\pi\,\frac{\Delta}{D_s}, \\ &\left[\nabla^2 \pm 2iQ\sin\alpha\frac{\partial}{\partial x} - Q^2\sin^2\alpha - \frac{2\omega}{D_s}\right] f_\pm^S = 0. \end{aligned} \tag{20}$$

As explained above, the x dependence has been dropped out in the transformed components $f_{s,\pm}$, so that we get

the equations in the S region

$$\left(\frac{\partial^2}{\partial z^2} - \frac{2\omega}{D_s}\right) f_s^S = -2\pi \frac{\Delta}{D_s},$$
$$\left[\frac{\partial^2}{\partial z^2} - Q^2 \sin^2\alpha - \frac{2\omega}{D_s}\right] f_\pm^S = 0, \quad (21)$$

and $f_{zz}^S = 0$, as it was also chosen in the ferromagnet. We may search the solutions for the triplet components $f_\pm^S$ satisfying the boundary condition (8) at the free interface $z = -d_s$ in the form:

$$f_\pm^S = C_\pm \frac{\cosh[k_s(z+d_s)]}{\sinh(k_s d_s)}, \quad (22)$$

with the wave vector $k_s = \sqrt{Q^2 \sin^2\alpha + 2\omega/D_s}$. The boundary conditions (9) at the SM interface ($z = 0$) read

$$\sum_i R_i V_+(k_i) + S_i U_+(k_i)\xi_f \gamma_c = 0,$$
$$\sum_i S_i V_-(k_i) + R_i U_-(k_i)\xi_f \gamma_c = 0, \quad (23)$$

where $\gamma_c = \gamma_b + \gamma \coth(k_s d_s)/\xi_s k_s$. For the singlet component, we finally get the two equations:

$$\frac{\partial}{\partial z} f_s^S(0) = -\gamma \frac{\xi_f}{\xi_s} \sum_i R_i k_i u_s(k_i),$$
$$f_s^S(0) = \sum_i S_i u_s(k_i) + \gamma_b R_i k_i u_s(k_i)\xi_f. \quad (24)$$

The latter equations can then be recasted in the form of the reduced boundary condition (10) with the expression (11) for the value of the quantity W. The coefficients R_i, S_i are determined by using Eqs. (18) and (23).

[1] D. S. Holmes *et. al.*, International Roadmap for devices and systems: 2018 Edition Cryogenic, Electronics and Quantum Information Processing, IEEE (2019).

[2] M. Eschrig, Spin-polarized supercurrents for spintronics, Phys. Today **64**, No. 1, 43 (2011).

[3] J. Linder and J. W. A. Robinson, Superconducting spintronics, Nat. Phys. **11**, 307 (2015).

[4] M. G. Blamire and J. W. A. Robinson, The interface between superconductivity and magnetism: understanding and device prospects, J. Phys. Condens. Matter **26**, 453201 (2014).

[5] M. Eschrig, Spin-polarized supercurrents for spintronics: a review of current progress, Rep. Prog. Phys. **78**, 104501 (2015).

[6] S. Oh, D. Youm, and M. R. Beasley, A superconductive magnetoresistive memory element using controlled exchange interaction, Appl. Phys. Lett. **71**, 2376 (1997).

[7] A. I. Buzdin, A. V. Vedyayev, and N. V. Ryzhanova, Spin-orientation-dependent superconductivity in F/S/F structures, Europhys. Lett. **48**, 686 (1999).

[8] L. R. Tagirov, Low-Field Superconducting Spin Switch Based on a Superconductor/Ferromagnet Multilayer, Phys. Rev. Lett. **83**, 2058 (1999).

[9] A. Singh, S. Voltan, K. Lahabi, and J. Aarts, Colossal Proximity Effect in a Superconducting Triplet Spin Valve Based on the Half-Metallic Ferromagnet CrO_2, Phys. Rev. X **5**, 021019 (2015).

[10] P. V. Leksin, N. N. Garif'yanov, A. A. Kamashev, A. A. Validov, Ya. V. Fominov, J. Schumann, V. Kataev, J. Thomas, B. Büchner, and I. A. Garifullin, Isolation of proximity-induced triplet pairing channel in a superconductor/ferromagnet spin valve, Phys. Rev. B **93**, 100502 (2016).

[11] N. O. Birge, A. E. Madden, and O. Naaman, Ferromagnetic Josephson junctions for cryogenic memory, Proc. SPIE **10732**, 107321M (2018).

[12] A. Vedyayev, C. Lacroix, N. Pugach, and N. Ryzhanova, Spin-valve magnetic sandwich in a Josephson junction, Europhys. Lett. **71**, 679 (2005).

[13] A. A. Golubov, M. Yu. Kupriyanov, Ya. V. Fominov, Critical current in SFIFS junctions, JETP Lett. **75**, 4, 190 (2002).

[14] N. O. Birge, Spin-triplet supercurrents in Josephson junctions containing strong ferromagnetic materials, Phil. Trans. R. Soc. A, **376**, No. 2125, 20150150 (2018).

[15] T. I. Larkin, V. V. Bol'ginov, V. S. Stolyarov, V. V. Ryazanov, I. V. Vernik, S. K. Tolpygo, and O. A. Mukhanov, Ferromagnetic Josephson switching device with high characteristic voltage, Appl. Phys. Lett. **100**, 222601 (2012).

[16] Y. V. Fominov, A. A. Golubov, and M. Y. Kupriyanov, Triplet proximity effect in FSF trilayers, JETP Letters **77**, 9, 510 (2003).

[17] Ya. V. Fominov, A. A. Golubov, T. Y. Karminskaya, M. Yu. Kupriyanov, R. G. Deminov, and L. R. Tagirov, Superconducting triplet spin valve, JETP Lett. **91**, 308 (2010).

[18] J. Y. Gu, C.-Y. You, J. S. Jiang, J. Pearson, Y. B. Bazaliy, and S. D. Bader, Magnetization-Orientation Dependence of the Superconducting Transition Temperature in the Ferromagnet-Superconductor-Ferromagnet System: CuNi/Nb/CuNi, Phys. Rev. Lett. **89**, 267001 (2002).

[19] A. Potenza and C. H. Marrows, Superconductor-ferromagnet CuNi/Nb/CuNi trilayers as superconducting spin-valve core structures, Phys. Rev. B **71**, 180503 (2005).

[20] K. Westerholt, D. Sprungmann, H. Zabel, R. Brucas, B. Hjorvarsson, D. A. Tikhonov, and I. A. Garifullin, Superconducting Spin Valve Effect of a V Layer Coupled to an Antiferromagnetic [Fe/V] Superlattice, Phys. Rev. Lett. **95**, 097003 (2005).

[21] R. Steiner and P. Ziemann, Magnetic switching of the superconducting transition temperature in layered ferromagnetic/superconducting hybrids: Spin switch versus stray field effects, Phys. Rev. B **74**, 094504 (2006).

[22] P. V. Leksin, A. A. Kamashev, N. N. Garif'yanov, I. A. Garifullin, Ya. V. Fominov, J. Schumann, C. Hess, V. Kataev, and B. Büchner, Peculiarities of performance of the spin valve for the superconducting current, JETP Lett. **97**, 478 (2013).

[23] M. G. Flokstra, T. C. Cunningham, J. Kim, N. Satchell, G. Burnell, P. J. Curran, S. J. Bending, C. J. Kinane, J. F. K. Cooper, S. Langridge, A. Isidori, N. Pugach, M. Eschrig, and S. L. Lee, Controlled suppression of superconductivity by the generation of polarized Cooper pairs in spin-valve structures, Phys. Rev. B **91**, 060501(R) (2015).

[24] F. S. Bergeret, A. F. Volkov, and K. B. Efetov, Josephson current in superconductor-ferromagnet structures with a nonhomogeneous magnetization, Phys. Rev. B **64**, 134506 (2001).

[25] A. Kadigrobov, R. I. Shekhter, and M. Jonson, Quantum spin fluctuations as a source of long-range proximity effects in diffusive ferromagnet-super conductor structures, Europhys. Lett. **54**, 394 (2001).

[26] M. Eschrig, J. Kopu, J. C. Cuevas, and Gerd Schön, Theory of Half-Metal/Superconductor Heterostructures, Phys. Rev. Lett. **90**, 137003 (2003).

[27] F. S. Bergeret, A. F. Volkov, and K. B. Efetov, Odd triplet superconductivity and related phenomena in superconductor-ferromagnet structures, Rev. Mod. Phys. **77**, 1321 (2005).

[28] P. V. Leksin, N. N. Garif'yanov, I. A. Garifullin, Y. V. Fominov, J. Schumann, Y. Krupskaya, V. Kataev, O. G. Schmidt, and B. Büchner, Evidence for Triplet Superconductivity in a Superconductor-Ferromagnet Spin Valve, Phys. Rev. Lett. **109**, 057005 (2012).

[29] P. Leksin, N. Garif'yanov, I. Garifullin, J. Schumann, H. Vinzelberg, V. Kataev, R. Klingeler, O. G. Schmidt, and B. Büchner, Full spin switch effect for the superconducting current in a superconductor/ferromagnet thin film heterostructure, Appl. Phys. Lett. **97**, 102505 (2010).

[30] B. Li, N. Roschewsky, B. A. Assaf, M. Eich, M. Epstein-Martin, D. Heiman, M. Müzenberg, and J. S. Moodera, Superconducting Spin Switch with Infinite Magnetoresistance Induced by an Internal Exchange Field, Phys. Rev. Lett. **110**, 097001 (2013).

[31] Y. Gu, G.Halasz, J. Robinson and M. Blamire, Large Superconducting Spin Valve Effect and Ultrasmall Exchange Splitting in Epitaxial Rare-Earth-Niobium Trilayers, Phys. Rev. Lett. **115**, 067201 (2015).

[32] A. A. Kamashev, A. A. Validov, J. Schumann, V. Kataev, B. Büchner, Y. V. Fominov, and I. A. Garifullin, Increasing the performance of a superconducting spin valve using a Heusler alloy, Beilstein J. Nanotechnol. **9**, 1764 (2018).

[33] U. D. Chacón Hernández, M. B. Fontes, E. Baggio-Saitovitch, M. A. Sousa, and C. Enderlein, Anti-Lenz Supercurrents in Superconducting Spin Valves, Phys. Rev. B **95**, 184509 (2017).

[34] T. E. Baker and A. Bill, The role of canting and depleted-triplet minima in superconducting spin valve structures, Phys. Rev. B **97**, 214520 (2018).

[35] E. Moen and O. T. Valls, Spin-split conductance and subgap peak in ferromagnet/superconductor spin valve heterostructures, Phys. Rev. B **98**, 104512 (2018).

[36] Z. Feng, J. W. A. Robinson, and Mark Blamire, Out of plane superconducting Nb/Cu/Ni/Cu/Co triplet spin-valves, Applied Physics Letters **111**, 042602 (2017).

[37] D. Lenk, R. Morari, V. Zdravkov, and R. Tidecks, Full-switching FSF-type superconducting spin-triplet magnetic random access memory element, Physical Review B **96**, 184521 (2017).

[38] N. V. Klenov, Yu. N. Khaydukov, S. V. Bakurskiy, I. I. Soloviev, R. Morari, T. Keller, M. Yu. Kupriyanov, A. S. Sidorenko, and B. Keimer, Periodic Co/Nb pseudo spin-valve for cryogenic memory, Beilstein J. Nanotechnol. **10**, 833 (2019).

[39] N. Banerjee, C. B. Smiet, R. G. J. Smits, A. Ozaeta, F. S. Bergeret, M. G. Blamire, and J. W. A. Robinson, Evidence for spin selectivity of triplet pairs in superconducting spin valves (Py-Ho-Nb-Ho-Py-FeMn), Nat. Commun. **5**, 3048 (2014).

[40] I. Sosnin, H. Cho, V. T. Petrashov, and A. F. Volkov, Superconducting Phase Coherent Electron Transport in Proximity Conical Ferromagnets, Phys. Rev. Lett. **96**, 157002 (2006).

[41] L. Y. Zhu, Y. Liu, F. S. Bergeret, J. E. Pearson, S. G. E. te Velthuis, S. D. Bader, and J. S. Jiang, Unanticipated Proximity Behavior in Ferromagnet-Superconductor Heterostructures with Controlled Magnetic Noncollinearity, Phys. Rev. Lett. **110**, 177001 (2013).

[42] F. Chiodi, J. D. S. Witt, R. G. J. Smits, L. Qu, G. B. Halász, C.-T. Wu, O. T. Valls, K. Halterman, J. W. A. Robinson, and M. G. Blamire, Supra-oscillatory critical temperature dependence of Nb-Ho bilayers, Europhys. Lett. **101**, 37002 (2013).

[43] Y. Gu, G. B. Halász, J. W. A. Robinson, and M. G. Blamire, Large Superconducting Spin Valve Effect and Ultrasmall Exchange Splitting in Epitaxial Rare-Earth-Niobium Trilayers, Phys. Rev. Lett. **115**, 067201 (2015).

[44] A. Di Bernardo, S. Diesch, Y. Gu, J. Linder, G. Divitini, C. Ducati, E. Scheer, M. G. Blamire, and J. W. A. Robinson, Signature of magnetic-dependent gapless odd frequency states at superconductor/ferromagnet interfaces, Nat. Commun. **6**, 8053 (2015).

[45] N. Satchell, J. D. S. Witt, M. G. Flokstra, S. L. Lee, J. F. K. Cooper, C. J. Kinane, S. Langridge, and G. Burnell, Control of Superconductivity with a Single Ferromagnetic Layer in Niobium/Erbium Bilayers, Phys. Rev. Appl. **7**, 044031 (2017).

[46] I. V. Vernik, V. V. Bol'ginov, S. V. Bakurskiy, A. A. Golubov, M. Yu. Kupriyanov, V. V. Ryazanov, and O. A. Mukhanov, Magnetic Josephson Junctions With Superconducting Interlayer for Cryogenic Memory, IEEE Trans. Appl. Supercond. **23**, 1701208 (2013).

[47] N. G. Pugach, M. Safonchik, T. Champel, M. E. Zhitomirsky, E. Lahderanta, M. Eschrig, and C. Lacroix, Superconducting spin valves controlled by spiral reorientation in B20-family magnets, Appl. Phys. Lett. **111**, 162601 (2017).

[48] N. A. Gusev, D. I. Dgheparov, N. G. Pugach, and V. I. Belotelov, Magnonic control of the superconducting spin valve by magnetization reorientation in a helimagnet, Appl. Phys. Lett. **118**, 232601 (2021).

[49] Y. Ishikawa, G. Shirane, J. A. Tarvin, and M. Kohgi, Magnetic excitations in the weak itinerant ferromagnet MnSi, Phys. Rev. B **16**, 4956 (1977).

[50] C. Pfleiderer, S. R. Julian, and G. G. Lonzarich, Non-

Fermi-liquid nature of the normal state of itinerant-electron ferromagnets, Nature **414**, 427 (2001).
[51] M. Uchida, Y. Onose, Y. Matsui, and Y. Tokura, Real-Space Observation of Helical Spin Order, Science **311**, 359 (2006).
[52] S. V. Grigoriev, S. V. Maleyev, V. A. Dyadkin, D. Menzel, J. Schoenes, and H. Eckerlebe, Principal interactions in the magnetic system $Fe_{1-x}Co_xSi$: Magnetic structure and critical temperature by neutron diffraction and SQUID measurements, Phys. Rev. B **76**, 092407 (2007).
[53] V. Dyadkin, S. V. Grigoriev, D. Menzel, D. Chernyshov, V. Dmitriev, J. Schoenes, S. V. Maleyev, E. V. Moskvin, and H. Eckerlebe, Control of chirality of transition-metal monosilicides by the Czochralski method, Phys. Rev. B **84**, 014435 (2011).
[54] S. Mühlbauer, B. Binz, F. Jonietz, C. Pfleiderer, A. Rosch, A. Neubauer, R. Georgii, and P. Böni, Skyrmion Lattice in a Chiral Magnet, Science **323**, 915 (2009).
[55] A. Fert, V. Cros, and J. Sampaio, Skyrmions on the track, Nature Nanotech. **8**, 152 (2013).
[56] D. Menzel, D. Schroeter, N. Steinki, S. Süllow, A. Fernández Scarioni, H. W. Schumacher, H. Okuyama, H. Hidaka, and H. Amitsuka, Hall effect and resistivity in epitaxial MnSi thin films under ambient and high pressure, IEEE Trans. Magn. **55**, 1500204 (2019).
[57] T. Champel and M. Eschrig, Switching superconductivity in superconductor/ferromagnet bilayers by multiple-domain structures, Phys. Rev. B **71**, 220506(R) (2005).
[58] T. Champel and M. Eschrig, Effect of an inhomogeneous exchange field on the proximity effect in disordered superconductor-ferromagnet hybrid structures, Phys. Rev. B **72**, 054523 (2005).
[59] A. F. Volkov, A. Anishchanka, and K. B. Efetov, Odd triplet superconductivity in a superconductor/ferromagnet system with a spiral magnetic structure, Phys. Rev. B **73**, 104412 (2006).
[60] G. B. Halász, J. W. A. Robinson, J. F. Annett, and M. G. Blamire, Critical current of a Josephson junction containing a conical magnet, Phys. Rev. B **79**, 224505 (2009).
[61] G. B. Halász, M. G. Blamire, and J. W. A. Robinson, Magnetic-coupling-dependent spin-triplet supercurrents in helimagnet/ferromagnet Josephson junctions, Phys. Rev. B **84**, 024517 (2011).
[62] C.-T. Wu, O. T. Valls, and K. Halterman, Proximity effects in conical-ferromagnet/superconductor bilayers, Phys. Rev. B **86**, 184517 (2012).
[63] K. Halterman and M. Alidoust, Half-metallic superconducting triplet spin valve, Phys. Rev. B **94**, 064503 (2016).
[64] A. A. Jara, C. Safranski, I. N. Krivorotov, C.-T. Wu, A. N. Malmi-Kakkada, O. T. Valls, and K. Halterman, Angular dependence of superconductivity in superconductor/spin-valve heterostructures, Phys. Rev. B **89**, 184502 (2014).
[65] Note that for itinerant electrons a similar magnetic texture appears in a metal with intrinsic spin-orbit interaction [66, 67]. By finding a way to control intrinsic spin-orbit interaction one may be able to explore such a spin-valve structure like a Josephson junction with a two-dimensional electron gas.
[66] I. V. Bobkova, A. M. Bobkov, and M.A. Silaev, Generalized quasiclassical theory of the long-range proximity effect and spontaneous currents in superconducting heterostructures with strong ferromagnets, Phys. Rev. B **96**, 094506 (2017).
[67] F. S. Bergeret and I. V. Tokatly, Spin-orbit coupling as a source of long-range triplet proximity effect in superconductor-ferromagnet hybrid structures, Phys. Rev. B **89**, 134517 (2014).
[68] T. Champel, T. Löfwander, and M. Eschrig, $0-\pi$ Transitions in a Superconductor/Chiral Ferromagnet/Superconductor Junction Induced by a Homogeneous Cycloidal Spiral, Phys. Rev. Lett. **100**, 077003 (2008).
[69] M. Yu. Kuprianov and V. F. Lukichev, Influence of boundary transparency on the critical current of "dirty" SS'S structures, Zh. Eksp. Teor. Fiz. **94**, 139 (1988) [Sov. Phys. JETP **67**, 1163 (1988)].
[70] Ya. V. Fominov, N. M. Chtchelkatchev, and A. A. Golubov, Nonmonotonic critical temperature in superconductor/ferromagnet bilayers, Phys. Rev. B **66**, 014507 (2002).
[71] T. Löfwander, T. Champel, and M. Eschrig, Phase diagrams of ferromagnet-superconductor multilayers with misaligned exchange fields, Phys. Rev. B **75**, 014512 (2007).
[72] M. Janoschek, M. Garst, A. Bauer, P. Krautscheid, R. Georgii, P. Boni and C. Pfleiderer, Fluctuation-induced first-order phase transition in Dzyaloshinskii-Moriya helimagnets, Phys. Rev. B **87**, 134407 (2013).
[73] A. Bauer, talk at DPG Spring Meeting, Berlin, March 11-16, (2018).
[74] A. Neubauer, C. Pfleiderer, B. Binz, A. Rosch, R. Ritz, P. G. Niklowitz, and P. Böni, Topological Hall Effect in the A Phase of MnSi, Phys. Rev. Lett. **102**, 186602 (2009).
[75] Y. Li, N. Kanazawa, X. Z. Yu, A. Tsukazaki, M. Kawasaki, M. Ichikawa, X. F. Jin, F. Kagawa, and Y. Tokura, Robust Formation of Skyrmions and Topological Hall Effect Anomaly in Epitaxial Thin Films of MnSi, Phys. Rev. Lett. **110**, 117202 (2013).
[76] T. L. Monchesky, Skyrmions: Detection with unpolarized currents, Nat. Nanotech. **10**, 1008 (2015).
[77] A. Tonomura, X. Z. Yu, K. Yanagisawa, T. Matsuda, Y. Onose, N. Kanazawa, H. S. Park, and Y. Tokura, Real-Space Observation of Skyrmion Lattice in Helimagnet MnSi Thin Samples, Nano Lett. **12**, 1673 (2012).
[78] M. Mochizuki, X. Z. Yu, S. Seki, N. Kanazawa, W. Koshibae, J. Zang, M. Mostovoy, Y. Tokura, and N. Nagaosa, Thermally driven ratchet motion of a skyrmion microcrystal and topological magnon Hall effect, Nature Materials **13**, 241 (2014).
[79] X. Yu, A. Kikkawa, D. Morikawa, K. Shibata, Y. Tokunaga, Y. Taguchi, and Y. Tokura, Variation of skyrmion forms and their stability in MnSi thin plates, Phys. Rev. B **91**, 054411 (2015).
[80] N. G. Pugach, M. Yu. Kupriyanov, E. Goldobin, R. Kleiner, and D. Koelle, Superconductor-insulator-ferromagnet-superconductor Josephson junction: From the dirty to the clean limit, Phys. Rev. B **84**, 144513 (2011).
[81] N. G. Pugach, M. Yu. Kupriyanov, A. V. Vedyayev, C. Lacroix, E. Goldobin, D. Koelle, R. Kleiner, and A. S. Sidorenko, Ferromagnetic Josephson junctions with step-like interface transparency, Phys. Rev. B **80**, 134516 (2009).
[82] J. Grefe, *Proximity-Effekte in Nb-B20-Heterostrukturen*, Bachelor thesis, Braunschweig Technical University, (2018).